Proceedings of ASME Turbo Expo 2011
GT2011
June 6-10, 2011, Vancouver, British Columbia, Canada

GT2011-46089

COMPRESSOR FOULING MODELING: RELATIONSHIP BETWEEN COMPUTATIONAL ROUGHNESS AND GAS TURBINE OPERATION TIME

Francesco Melino
IMEM – CNR
Parma, Italy

Mirko Morini
MechLav - Università di Ferrara
Ferrara, Italy

Antonio Peretto
DIEM - Università di Bologna
Bologna, Italy

Michele Pinelli
Dipartimento di Ingegneria - Università di Ferrara
Ferrara, Italy

Pier Ruggero Spina
Dipartimento di Ingegneria - Università di Ferrara
Ferrara, Italy

ABSTRACT

Gas turbine axial compressor performance is heavily influenced by blade fouling; as a result, the gas turbines efficiency and producible power output decrease.

Performance degradation of an axial compressor stage due to fouling can be analyzed by means of simulation through Computational Fluid Dynamics (CFD) codes. Usually these methods reproduce the deteriorated blades by increasing their surface roughness and/or thickness [1].

Another approach is the scaling of compressor stage performance maps. A model based on stage-by-stage techniques was presented in a previous work. This model is able to estimate the modifications of the overall compressor performance map as a function of the operating hours [2].

The aim of the present study is to combine these two different approaches in order to relate the increase of blade computational surface roughness with compressor operating hours.

NOMENCLATURE

C	constant
C_μ	model constant
h	total enthalpy
k	turbulent kinetic energy
k_s	equivalent sand grain
k^+	non-dimensional roughness height
$\tilde{k}^+$	modified non-dimensional roughness height
M	mass flow rate
R_a	Center Line Average (CLA) roughness
Re_k	roughness Reynolds number
SF	shape factor
t	time, hours
T	temperature
U	blade velocity at mean radius
u_t	velocity tangent to the wall
u^+	non-dimensional velocity
$\tilde{u}_\tau$	modified friction velocity
V_X	axial flow velocity
W	relative velocity
y	normal distance, cartesian coordinate
y^+	non-dimensional distance
$\tilde{y}^+$	modified non-dimensional distance
β	compressor or stage pressure ratio
γ	fouling scaling coefficient
$\phi = \frac{V_X}{U}$	flow coefficient
κ	model constant, Eq. (6)
μ	dynamic viscosity
ν	kinematic viscosity
η	compressor or stage efficiency
$\psi_p = \frac{\Delta h_{stage}}{U^2}$	pressure coefficient

Subscripts and superscripts

AIR	air
DES	relative to design conditions
FOU	relative to fouled conditions
P	referred to near-wall node
stage	compressor stage
0	relative to new and clean conditions
*	normalized to design value

Acronyms

CFD	Computational Fluid Dynamics
IN.FO.G.T.E	INterstage FOgging Gas Turbine Evaluation

INTRODUCTION

Environmental conditions of the site in which a gas turbine or a combined cycle power plant are installed strongly influence their performance. In particular, compressor fouling, which is one of the main reasons for gas turbine compressor performance degradation, is heavily influenced by the quality of the air swallowed by the compressor. It is estimated that, typically, compressor fouling accounts for 70 % to 85 % of the total gas turbine performance loss during continuous operation [3].

The effect of compressor fouling is the reduction of the inlet air mass flow rate, isentropic efficiency and pressure ratio. These influence the coupling between the compressor and turbine and result in a loss of the gas turbine power output and overall efficiency. The loss of the gas turbine power output can range from 2 % under favorable conditions, to (15-20) % under adverse conditions [4].

Axial compressor fouling is caused by the adherence of small particles to blades surfaces; this causes an increase of blade roughness and, as a consequence, a change in the shape of the airfoil.

In spite of the presence of the filters in the inlet duct, the particles can reach the axial compressor due to their small diameter, which is generally smaller than (2-10) μm [5]; usually these particles can be removed by adequate compressor washing.

In recent years, many Authors have studied this matter, describing the gas turbine performance degradation mechanisms [3-8], developing analytical models [9-11] and focusing on diagnostics and maintenance aspects [12, 13].

The aim of this study is to combine two different approaches in order to estimate the performance degradation of a compressor stage due to fouling, and to understand the relationship between compressor operating hours and the increase in blade computational surface roughness. The first approach provides the performance changes due to fouling of an actual compressor stage through CFD simulations [1]. The second approach makes it possible to estimate the overall compressor performance map modifications due to fouling as a function of operating hours. This approach uses a compressor stage-by-stage model and a scaling technique of the compressor stage performance maps and is included in the IN.FO.G.T.E. code [14], which was tuned according to results available in literature [2].

AXIAL COMPRESSOR FOULING MODELING

CFD model. In order to investigate the effects of fouling on a compressor stage, the NASA Stage 37 test case was used as the baseline geometry. The geometry and performance data were gathered from [15]. The entire compressor stage (rotor and stator) was simulated.

<u>Reference compressor stage.</u> The NASA Stage 37 is composed of a rotor and a stator. Multiple Circular Arc blade profiles were used in the original design for all blade rows. The overall NASA Stage 37 performance at the design point (corrected mass flow of 20.19 kg/s and rotational speed of 17,188 rpm) is a pressure ratio equal to 2.050 and an adiabatic efficiency equal to 0.842. The rotor is composed of 36 blades and is characterized by an inlet hub-to-tip diameter ratio of 0.7, a blade aspect ratio of 1.19 and a tip solidity of 1.29. The tip clearance at design speed is 0.356 mm (0.45 % of the blade span). The Rotor design pressure ratio and adiabatic efficiency are 2.106 and 0.877 and the design tip speed is 454 m/s, respectively. The stator is composed of 46 blades. Its blade aspect ratio is equal to 1.26 and its tip solidity is equal to 1.3.

<u>Geometric assumptions.</u> To reduce computational effort, only a section of the full geometry was modeled. Due to the impossibility of an ideal periodicity that could match both rotor and stator, the computational domain consisted of 4 rotor blades and 5 stator blades. This resulted in a 40.00° section for the rotor and a 39.13° section for the stator. This also resulted in a rotor/stator pitch ratio at the interface equal to 1.250 instead of 1.278 of the real geometry.

In Fig. 1, a sketch of the computational domain is reported.

The simulations were performed in a steady multiple frame of reference taking into account the contemporary presence of moving and stationary domains by means of a mixing plane approach imposed at the rotor/stator interface (which was located half-way between the two components).

<u>Numerical grid.</u> The grids used in the calculations were hybrid grids generated by means of ANSYS ICEM CFD 11.0 [16]. The grids were realized by starting from a tetrahedral mesh and then by adding prism layers on the surface of the blades to help solve the boundary layer around the blade. The final mesh was composed of about 1,055,000 elements and 9 prism layers (Fig. 1) and the first grid point height was fixed at 50 μm: this choice makes it possible to correctly solve the boundary layers for the roughened wall in the considered range of roughness k_s = (1-30) μm [17].

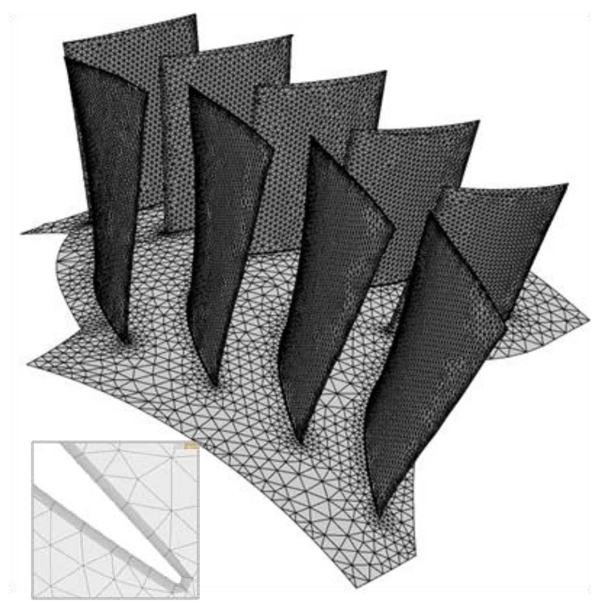

Figure 1 – Modeled geometry, numerical grid and detail of the prism layer near the blade surface for NASA Stage 37

Numerical issues. The numerical simulations were carried out with the commercial CFD code ANSYS CFX 11.0 [18]. The code solves the 3D Reynolds-averaged form of the Navier–Stokes equations by using a finite-element based finite-volume method. An Algebraic Multigrid method based on the Additive Correction Multigrid strategy was used. A second-order high-resolution advection scheme was adopted to calculate the advection terms in the discrete finite-volume equations.

The turbulence models used in the calculations is the standard k-ε model. Near-wall effects are modeled by means of scalable wall functions in the k-ε model, which means that the model uses empirical formulas that impose suitable conditions near the wall without resolving the boundary layer. In particular, scalable wall functions are based on the analytical-wall-function approach (well documented in [19]), in which a modified turbulent velocity scale $\tilde{u}_\tau$ dependent on the turbulent kinetic energy at the near-wall node k_P is used

$$\tilde{u}_\tau = C_\mu^{1/4} k_P^{1/2} \tag{1}$$

and, as a consequence, a modified y^+ based on $\tilde{u}_\tau$ can be obtained:

$$\tilde{y}^+ = \tilde{u}_\tau y / \nu \tag{2}$$

The basic idea behind the scalable wall-function approach is to limit the computed $\tilde{y}^+$ value used in the logarithmic formulation from falling below 11.06, which is the value assumed for the intersection between the logarithmic and the linear near wall profile [18].

In order to account for surface roughness of deteriorated blades, the near-wall model of the k-ε turbulence model has to be modified. For rough walls, the logarithmic profile still exists, but moves closer to the wall. As an index of the wall roughness, the equivalent sand grain k_s is used.

Roughness effects can be accounted for by modifying the logarithmic profile as follows:

$$u^+ = \frac{u_t}{u_\tau} = \frac{1}{\kappa}\ln\left(\frac{\tilde{y}^+}{1 + 0.3\cdot\tilde{k}^+}\right) + C \tag{3}$$

where

$$\tilde{k}^+ = \frac{k_s \tilde{u}_\tau}{\nu} \tag{4}$$

Equations (3) and (4) are coherent with the scalable wall functions definition.

Boundary conditions. The total pressure, total temperature and flow angle were imposed at the inflow boundary. The inlet total pressure and total temperature were fixed at p_{01} = 101,325 Pa and T_{01} = 288.15 K, respectively.

Regarding outflow boundary conditions, two different strategies were followed depending on the zone of the (M, β) performance map where the working point to be simulated is located. In fact, the slope of the curve is different when near-stall or near-choked flow regions are attained and, as a consequence, (i) an average relative static pressure p_{r2} was imposed at the outflow boundary in the near-choked flow region and (ii) a mass flow rate was imposed at the outflow boundary in the near-stall region.

The imposed angular velocity refers to the working conditions at 100 % design speed [15]. Therefore, the imposed rotational speed for the calculations was set as n = 17,197 rpm.

Roughness was considered uniform along all the blade surface and an equivalent sand grain roughness k_s value was set on the pressure and suction surfaces of the rotor and stator blades as in Tab. 1. Although in real engines the surface roughness is usually not uniform, it was thought that simple tests with uniform roughness will be useful in exploring the significance of surface roughness itself [1]. To relate R_a and k_s the correlation of Koch and Smith [20] has been used, i.e. k_s = 6.2 R_a.

Finally, since only a section of the full geometry was modeled, rotational periodic boundary conditions were applied to the lateral surfaces of the flow domain.

Model validation. In [1], a validation of the numerical model was performed and confirmed that:

(i) the shapes of all the experimental performance maps is correctly reproduced by the numerical code, and the error between the calculated and measured values of the mass flow is about 1.4 % in the choked condition at 100 % rotational speed;

(ii) the differences between the design values of the performance parameters of the numerical model and the actual compressor stage are less than 2 %.

Thus, the numerical model was considered reliable.

Table 1 – Parameters for simulation

	k_s (μm)	R_a (μm)	k_s/c
CFD-S	1	0.16	$1.77\cdot10^{-5}$
CFD-R1	10	1.61	$1.77\cdot10^{-4}$
CFD-R2	15	2.42	$2.66\cdot10^{-4}$
CFD-R3	20	3.23	$3.54\cdot10^{-4}$
CFD-R4	25	4.03	$4.43\cdot10^{-4}$
CFD-R5	30	4.84	$5.31\cdot10^{-4}$

Modification of compressor performance maps due to fouling through the scaling method. The performance of a fouled axial compressor stage was simulated by means of the following equations [2]:

$$\psi_p = \psi_{p,max} + - \frac{\left(\psi_{p,max} - \psi_{p,FOU}\right)\cdot\left[\phi_{\psi_{p,max}} + SF\cdot\left(\phi_{\psi_{p,max}} - \phi_{FOU}\right) - \phi\right]^2}{\left[\phi_{\psi_{p,max}} + SF\cdot\left(\phi_{\psi_{p,max}} - \phi_{FOU}\right) - \phi_{FOU}\right]^2} \tag{5}$$

$$\begin{cases} \dfrac{\Psi_p}{\phi} \in \left[\left(\dfrac{\Psi_p}{\phi}\right)_{min}, \dfrac{\Psi_{p,FOU}}{\phi_{FOU}}\right] \\ \eta = \eta_{FOU} + \\ -\dfrac{\eta_{FOU}-\eta_{(\Psi_p/\phi)_{min}}}{\left[\dfrac{\Psi_{p,FOU}}{\phi_{FOU}} - \left(\dfrac{\Psi_p}{\phi}\right)_{min}\right]^{3.5}} \left(\dfrac{\Psi_{p,FOU}}{\phi_{FOU}} - \dfrac{\Psi_p^*}{\phi^*}\right)^{3.5} \end{cases} \tag{6}$$

$$\begin{cases} \dfrac{\Psi_p}{\phi} \in \left[\dfrac{\Psi_{p,FOU}}{\phi_{FOU}}, \left(\dfrac{\Psi_p}{\phi}\right)_{max}\right] \\ \eta^* = \eta_{FOU} + \\ -\dfrac{\eta_{FOU}-\eta_{(\Psi_p/\phi)_{max}}}{\left[\left(\dfrac{\Psi_p}{\phi}\right)_{max} - \dfrac{\Psi_{p,FOU}}{\phi_{FOU}}\right]^{2}} \left(\dfrac{\Psi_p}{\phi} - \dfrac{\Psi_{p,FOU}}{\phi_{FOU}}\right)^{2} \end{cases} \tag{7}$$

$$\begin{cases} \phi_{FOU} = \gamma_\phi \cdot \phi_{DES} \\ \Psi_{P,FOU} = \gamma_\Psi \cdot \Psi_{P,DES} \\ \eta_{FOU} = \gamma_\eta \cdot \eta_{DES} \end{cases} \tag{8}$$

where γ_Ψ, γ_ϕ, $\gamma_\eta \in [0,1]$, and γ_Ψ, γ_ϕ, $\gamma_\eta = 1$ means that the compressor stage is in clean conditions, while γ_Ψ, γ_ϕ, $\gamma_\eta < 1$ means a fouled compressor stage. The coefficients γ_Ψ, γ_ϕ, γ_η depend on the operating time, i.e. :

$$\begin{cases} \gamma_\phi = F_\phi(t) \\ \gamma_\Psi = F_\Psi(t) \\ \gamma_\eta = F_\eta(t) \end{cases} \tag{9}$$

where "t" is the time passed since the last compressor washing; the functions $F_\Psi(t)$, $F_\phi(t)$, $F_\eta(t)$, can be defined by a tuning procedure as better explained in [2].

The equations from 5 to 9 allow the calculation of pressure coefficient (Ψ_p) and the total to total isentropic efficiency (η) in the current stage conditions as a function of flow coefficient (ϕ), Shape Factor (SF) and ratio Ψ_p/ϕ, once the design performance (ϕ_{DES}, $\Psi_{p,DES}$ and η_{DES}) and time since the last compressor washing are known.

Figures 2 and 3 highlight the changes of the stage pressure coefficient curve $\Psi_p = F_\Psi(\phi, SF)$ and efficiency curve $\eta = F_\eta(\Psi_p/\phi)$ respectively, as a function of γ_Ψ and γ_ϕ; the $\Psi_p = F_\Psi(\phi, SF)$ curve, in particular, refers to SF = 0 (subsonic stage).

In order to consider that fouling decreases moving from the first to the last stage of a multistage compressor, the functions $F_{\gamma\Psi}(i)$, $F_{\gamma\phi}(i)$ and $F_{\gamma\eta}(i)$ were introduced. They make it possible to estimate coefficients γ_Ψ, γ_ϕ and γ_η of each compressor stage as a function of the ones of the first stage. Therefore, the performance deterioration of the overall multistage compressor as a function of operating hours is known if γ_Ψ, γ_ϕ and γ_η for the first stage and $F_{\gamma\Psi}(i)$, $F_{\gamma\phi}(i)$ and $F_{\gamma\eta}(i)$ are known. More details on this scaling technique can be found in [2].

The tuning of the model was carried out by considering the following trends as a function of the operating hours [21]: compressor efficiency (η_{FOU}/η_0), inlet mass flow rate ($M_{AIR,FOU}/M_{AIR,0}$) and pressure ratio (β_{FOU}/β_0). The tuning phase made it possible to find, by trial and error procedure, γ_Ψ, γ_ϕ and γ_η of the first compressor stage as a function of the operating hours and the functions $F_{\gamma\Psi}(i)$, $F_{\gamma\phi}(i)$ and $F_{\gamma\eta}(i)$, in order to reproduce the trends reported in [21].

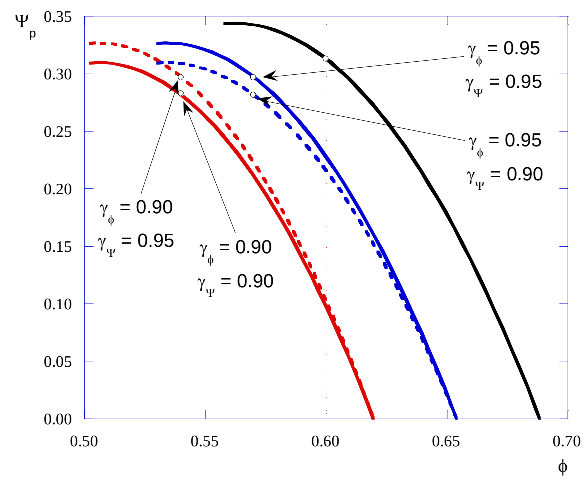

Figure 2 – Influence of fouling coefficients (γ_Ψ, γ_ϕ, γ_η) on the stage pressure coefficient curve (SF = 0: subsonic stage)

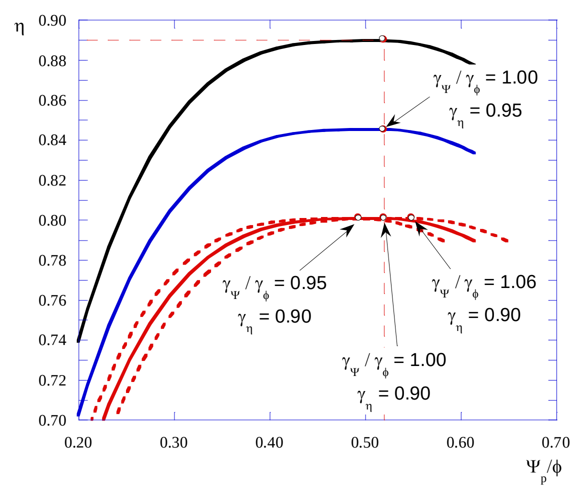

Figure 3 – Influence of fouling coefficients (γ_Ψ, γ_ϕ, γ_η) on the stage efficiency curve (SF=-0.5)

In Fig. 4 the comparison between literature data (continuous line) and IN.FO.G.T.E. calculations (circle and triangle markers) is presented.

The small errors and standard deviations between IN.FO.G.T.E. calculations after the tuning procedure and literature data reported in Tab. 2 indicate a satisfactory calibration of the model.

Figure 5 presents γ_Ψ, γ_ϕ and γ_η trends for the first compressor stage as a function of the operating hours as obtained by the tuning procedure.

It should be observed that this scaling technique makes it possible to relate the change of axial stage compressor performance maps with the machine operating hours.

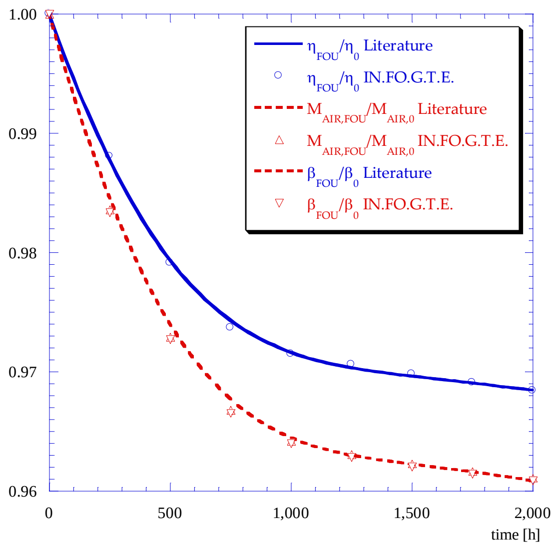

Figure 4 – Comparison between literature data and IN.FO.G.T.E. calculation

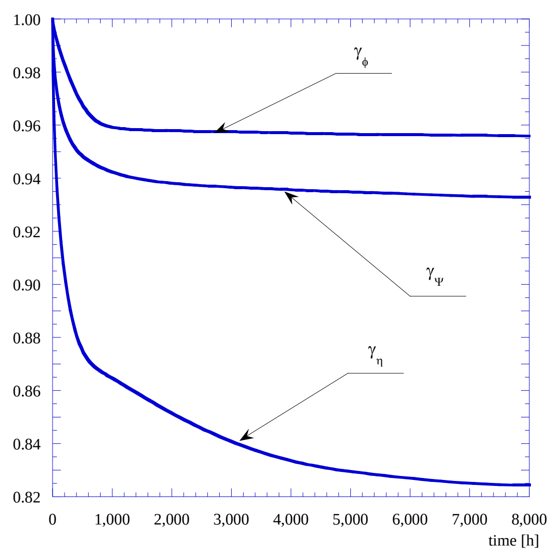

Figure 5 – Fouling coefficient as function of time

Table 2 – Comparison between literature data and IN.FO.G.T.E. calculation

	$\frac{\eta_{FOU}}{\eta_0}$	$\frac{M_{AIR,FOU}}{M_{AIR,0}}$	$\frac{\beta_{FOU}}{\beta_0}$
max absolute error [%]	0.051	0.090	0.113
average error [%]	-0.005	0.024	0.045
standard deviation [%]	0.028	0.048	0.049

MODEL COMPARISON

This section presents the comparison between the change of the axial compressor stage performance curves due to fouling as evaluated in [1] by CFD calculations and as calculated in [2] by means of the scaling method. More in detail, the design values of the flow coefficient, pressure coefficient, total to total isentropic efficiency and shape factor were found and used in Eqs from 5 to 7 in order to fit the NASA Stage 37 performance curves in the case of new and clean conditions (which means γ_Ψ, γ_ϕ, γ_η = 1). Then, the scaling technique was applied by trial and error to determinate the number of operating hours allowing the curve to fit the performance estimated by CFD for four selected values of k_s. The main result of this analysis is the determination of a relationship between the compressor operating hours and the increase in the computational blade surface roughness.

Figures 6 and 7 show the results of this analysis in terms of tuning of the scaling model with the CFD simulated performance maps. Data gathered from CFD simulations are reported by means of white circle markers, while the blue line represents the scaled performance map.

As already highlighted in [1] by adding roughness to the blade surfaces, (Ψ_p, ϕ) curve (Fig. 6) moves towards lower values of both flow and pressure coefficients. Moreover, the isentropic efficiency (Fig. 7) also decreases.

The generalized pressure coefficient stage performance curve perfectly fits the CFD points, both for the smooth stage and roughened stages. Regarding, the efficiency curve, it can be highlighted that the generalized stage performance cannot correctly represent the NASA Stage 37. The agreement between the generalized curve and the CFD points can only be considered satisfactory close to the design point. This is mainly due to the fact that the generalized efficiency curve was fitted to experimental measurements and calculated data of subsonic stages [22], while NASA Stage 37 is a transonic stage [15].

Concerning the capability of the time-degradation model to catch the reduction of the performance parameters due to the added roughness, it can be highlighted that, also in this case, the model perfectly fits the pressure coefficient curves. The value of the maximum efficiency is also correctly predicted up to k_s = 20 μm, while the scaling model overestimate the reduction of the maximum efficiency due to fouling for further increases. This is probably due to the fact that the scaling method was tuned on an axial compressor with subsonic

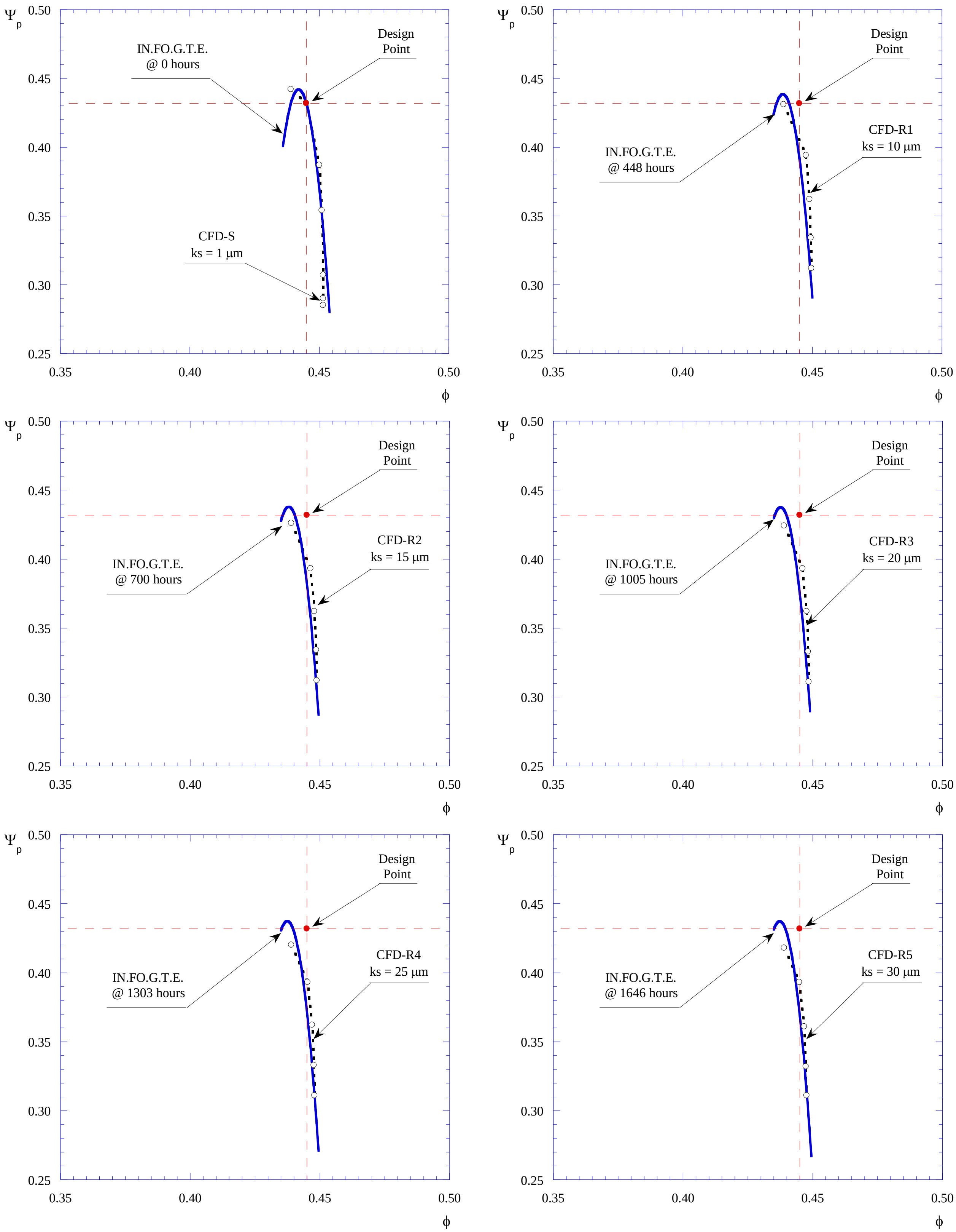

Figure 6 – Comparison between the change of NASA Stage 37 performance curve (pressure coefficient versus flow coefficient) due to fouling as evaluated by CFD method and scaling method

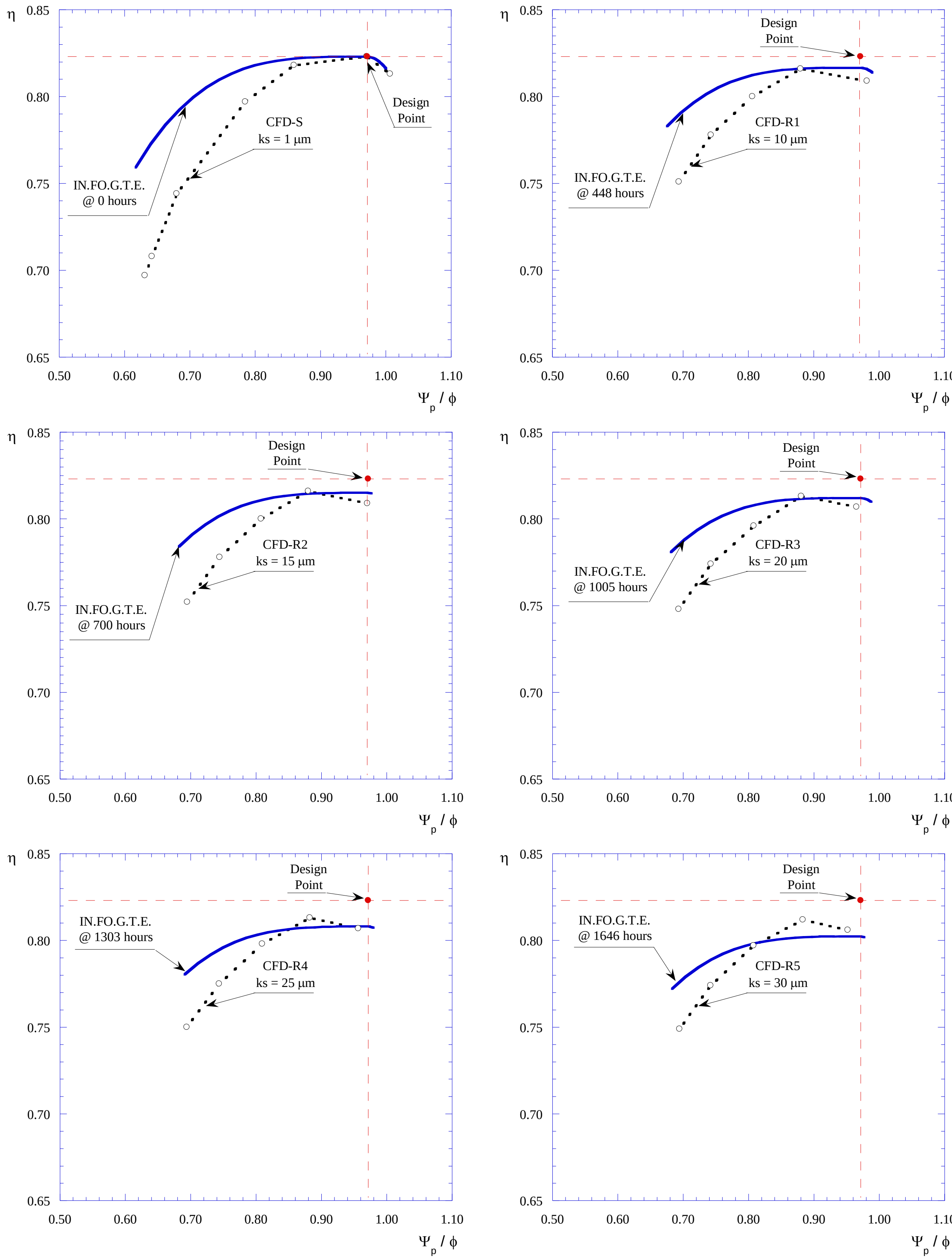

Figure 7 – Comparison between the change of NASA Stage 37 performance curve (total to total isentropic efficiency versus pressure to flow coefficient ratio) due to fouling as evaluated by CFD method and scaling method

stages [21], which may be characterized by a different behavior when severe fouled conditions are achieved.

Figures 6 and 7 also report the values of the operating hours necessary for the stage to reach this state of degradation. This information is also summarized in Fig. 8. As expected, it takes a longer time to reach higher levels of degradation (and, therefore, higher values of roughness). Nevertheless, the trend is not linear: this is in accordance with the model and in particular with the functions in Fig. 4 and Fig. 5.

METHOD APPLICATION TO A MULTISTAGE COMPRESSOR

The method developed has been applied to a multistage compressor in order to define the state of each stage in terms of computational roughness as a function of the operating hours. The compressor considered is a seventeen-stage axial flow compressor with a pressure ratio of about 12.5. The results are reported in Fig. 9. It can be observed that the magnitude of the added computational roughness decreases in a nonlinearly manner from the first to the last stage, while it increases by increasing the operating hours.

In turbomachinery calculations, Koch and Smith [20] proposed a method (originally theorized by Schlichting [23]) to distinguish between the hydraulically smooth regime and rough regimes, based on the definition of roughness Reynolds number

$$Re_{\mathrm{k}} = \frac{k_{\mathrm{s}} W_1}{\nu} \qquad (9),$$

where W_1 is the relative inlet velocity and ν is the cinematic viscosity of the fluid. This method states that a surface can be considered hydraulically smooth when Re_{k} is lower than 90. In the cases considered, this condition is verified for an equivalent sand grain k_{s} lower than 5 μm (a relative velocity W_1 equal to about 300 m/s can be assumed for the first stage).

Therefore, as can be observed from Fig. 9, up to 2000 operating hours the rough regime is verified only for the first stage. The other stages can be considered hydraulically smooth without affecting the compressor performance in a significant way. In the perspective of the computational fluid dynamics, it can be assumed that their effect is negligible, and, therefore, the roughness model can only be enabled for the stages that operate in the rough regime.

CONCLUSIONS

In this paper two different approaches for the estimation of the performance degradation of a compressor stage due to fouling have been combined, in order to understand the relationship between compressor operating hours and the increase in blade computational surface roughness. The first approach provides the performance changes due to fouling of an actual compressor stage through CFD simulations, while the second approach allows the estimation of the overall compressor performance map modification due to fouling as a function of operating hours by means of a scaling procedure.

The two methods have been applied to a compressor stage in order to correlate the increase in the blade surface roughness with the compressor stage operating hours.

The comparison between the two methods shows a good matching when the pressure coefficient curves are taken into account. Regarding the efficiency curves, the agreement can only be considered satisfactory close to the design point. This is mainly due to the fact that the generalized efficiency curve used by the scaling procedure was fitted to experimental measurements and calculated data of subsonic stages, while CFD calculations are performed on a transonic stage. Concerning the capability of the time-degradation model to catch the reduction of the efficiency due to the added computational roughness, it can be highlighted that the value of

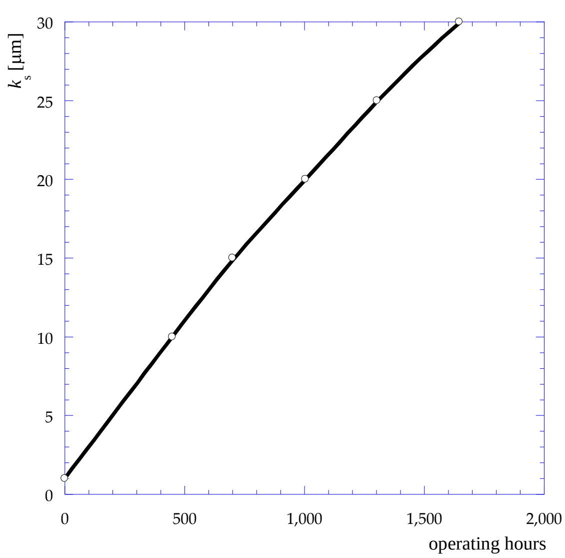

Figure 8 – Equivalent sand grain roughness as function of operating hours

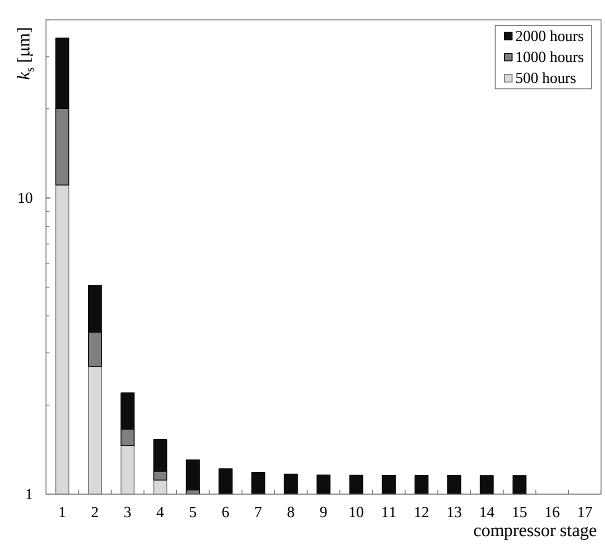

Figure 9 – Equivalent sand grain roughness for the different compressor stages

the maximum efficiency is also correctly predicted up to an equivalent sand grain roughness equal to 20 µm, while the scaling model overestimate efficiency reduction for further increases.

In any case, a relation between operating the time and blade roughness was found and applied to a multistage compressor: it was observed that there is a significant variation in computational roughness to be imposed in CFD simulations only after a certain amount of hours and only for the first stage.

REFERENCES

[1] Morini, M., Pinelli, M., Spina, P. R., Venturini, M., 2010, "Computational Fluid Dynamics Simulation of Fouling on Axial Compressor Stages", *ASME J. of Eng. Gas Turbines Power*, **132**, 072401 (10 pages).

[2] Melino, F., Peretto, A., Spina, P. R., 2010, "Development and Validation of a Model for Axial Compressor Fouling Simulation", ASME Paper GT2010-22947.

[3] Diakunchak, I., S., 1992, "Performance Deterioration in Industrial Gas Turbines", *ASME J. Eng. Gas Turbines Power*, **114**, pp. 161-168.

[4] Meher-Homji, C., B., Chaker, M., Bromley, A., F., 2009, "The Fouling Of Axial Flow Compressors – Causes, Effects, Susceptibility And Sensitivity", ASME Paper GT2009-59239

[5] Kurz, R., Brun, K., 2008, "Degradation of Gas Turbine Performance in Natural Gas Service", *J. Natural Gas Sci. Eng.*, **1**, pp. 95-102

[6] Meher-Homji, C. B., Chaker, M., Motiwalla, H., 2001, "Gas Turbine Performance Deterioration", Proceedings of the 30th Turbomachinery Symposium, Houston, Texas,USA.

[7] Meher-Homji, C. B., 1992, "Gas Turbine Axial Compressor Fouling - A Unified Treatment of its Effects, Detection and Control", *Int. J. Turbo and Jet Eng.*, **9**, pp 99-111.

[8] Meher-Homji, C.B., Bromley, A.F., 2004, "Gas Turbine Axial Compressor Fouling and Washing", Proceedings of the 33rd Turbomachinery Symposium, Texas A&M University, Houston, Texas, USA.

[9] Bammert, K., Woelk, G. U., 1980, "The Influence of Blading Surface Roughness on the Aerodynamic Behavior and Characteristic of an Axial Compressor", *ASME J. Eng. Gas Turbines Power*, **102**, pp. 283-287.

[10] Song, T. W., Sohn, J. L., Kim, T. S., Kim, J. H., Ro, S. T., 2003, "An Improved Analytic Model to Predict Fouling Phenomena in the Axial Compressor of Gas Turbine Engines", Proceedings of the International Gas Turbine Congress, Tokyo, Japan.

[11] Morini, M., Pinelli M., Spina, P. R., Venturini, M., 2010, "Influence of Blade Deterioration on Compressor and Turbine Performance", *ASME J. Eng. Gas Turbines Power*, **132**, 032401 (11 pages).

[12] Gulen, S. C., Griffin, P. R., Paolucci, S., 2002,"Real-Time On-Line Performance Diagnostics of Heavy-Duty Industrial Gas Turbines", *ASME J. Eng. Gas Turbines Power*, **124**, pp. 910-921.

[13] Srinivasa Rao, P. N., Achutha Naikan, V. N., 2008, "An Optimal Maintenance Policy for Compressor of a Gas Turbine Power Plant", *ASME J. Eng. Gas Turbines Power* , **130**, 021801 (5 pages).

[14] Bagnoli, M., Bianchi, M., Melino, F., Spina, P., R., 2008, "Development And Validation of a Computational Code for Wet Compression Simulation of Gas Turbines", *ASME J. Eng. Gas Turbines Power*, **130**, 012004 (8 pages).

[15] Reid, L., Moore, R. D., 1978, "Design and overall performance of four highly-loaded, high-speed inlet stages for an advanced high-pressure-ratio core compressor", NASA TP 1337.

[16] ICEM CFD 11.0, 2007, User Manual.

[17] Cadorin, M., Morini, M., Pinelli, M., 2010, "Numerical Analyses of High Reynolds Number Flow of High Pressure Fuel Gas Through Rough Pipes", *International Journal of Hydrogen Energy*, **35**, pp.7568-7579.

[18] ANSYS CFX 11.0, 2007, User Manual.

[19] Apsley, D., 2007, "CFD Calculation of Turbulent Flow with Arbitrary Wall Roughness", *Flow, Turbulence and Combustion*, **78**, pp. 153-175.

[20] Koch, C. C., Smith, L. H., 1976, ''Loss Sources and Magnitudes in Axial Flow Compressors,'' *ASME J. Eng. Gas Turbines Power*, **98**, pp. 411–424

[21] Tarabrin, A. P., Bodrov, A. I., Schurovsky, V. A. Stalder, J-P., 1998, "Influence of Axial Compressor Fouling on Gas Turbine Unit Performance Based on Different Schemes and with Different Initial Parameters", ASME Paper 98-GT-416.

[22] Howell, A. R., Bonham, R. P., 1950, "Overall and Stage Characteristics of Axial Flow Compressors", *Proc. IMechE*, **163**, pp. 235-248.

[23] Schlichting, H., 1960, "Boundary Layer Theory", *4th Edition*, McGraw-Hill, New York, USA.